Available online at www.sciencedirect.com
SCIENCE DIRECT
Remote Sensing of Environment 98 (2005) 80 – 95
Remote Sensing of Environment
www.elsevier.com/locate/rse

Variability of biome reflectance directional signatures as seen by POLDER

Cédric Bacour *, François-Marie Bréon

Laboratoire des Sciences du Climat et de l'Environnement, Commissariat à l'Energie Atomique, Gif-sur-Yvette, France

Received 21 January 2005; received in revised form 6 June 2005; accepted 9 June 2005

Abstract

Reflectance measurements acquired with the spaceborne POLDER instrument are used to analyze the variability of land surface directional signatures as a function of vegetation cover type. The reflectance directional signatures are quantified by the three parameters of a modified version of the Ross–Li reflectance model. The variability of the estimated parameters with respect to the seven MODIS biome classes was found to be higher within the classes than between classes, with the exception of the desert targets that show more isotropic reflectances. A limited number of standard BRDFs (typically 5 in the red and near infrared) capture most of the variability of the directional reflectance measurements, supporting the idea that different land surfaces have similar directional signatures. Over vegetation targets, they are characterized by a strong increase toward backscattering and much smaller variations in forward directions. The results express the diversity in structural situations within a given biome class and indicate that, at the resolution of the POLDER sensor, i.e. a few kilometers, the BRDF contains little information on the dominant vegetation type. We show that standard directional signatures may be used to correct the reflectance measurements for directional effects with an RMS error on the order of 0.011 in the red and 0.015 in the near infrared.

Keywords: Bidirectional reflectance distribution function; POLDER; Bidirectional effect normalization; Biome classification

1. Introduction

Reflectance measurements in the visible and near infrared (IR) spectral ranges are commonly used to monitor land-surfaces, including vegetation canopies, for quantifying changes in the Earth system or modeling its functioning. Classical biogeophysical variables that are estimated from the remote sensing data include the leaf area index (*LAI*) or the fraction of absorbed photosynthetically active radiation (*fAPAR*). A major difficulty for quantitative estimation of vegetation and soil characteristics from the reflectance measurements results from their anisotropy. For a given target, the reflectance varies as a function of sun and sensor geometry. The use of reflectance ratios lessens the anisotropic effects, as compared to individual measurements, because the directional signatures are similar in the various spectral bands. This explains in part the success of indices such as the NDVI (normalized difference vegetation index), up to recent years, for understanding the functioning and dynamics of the biosphere (Braswell et al., 1997; Maisongrande et al., 1995; Myneni et al., 1997). Simple vegetation indices however cannot be used for an accurate quantification of vegetation cover and photosynthetic activity because they do not directly relate to such intrinsic vegetation characteristics. There is a need to fully use the individual reflectance measurements, which requires a correction of their directional variations (Leroy & Roujean, 1994). Traditionally, time series of satellite measurements have been used to evaluate and correct the anisotropy (Cihlar et al., 1997; d'Entremont et al., 1999; Duchemin, 1999; Wu et al., 1995) although with a very limited sampling of the BRDF (Bidirectional Reflectance Distribution Function). Such sampling provided by cross-track scanners such as AVHRR (Advanced Very High Resolution Radiometer) or VEGETATION is not sufficient to properly assess the anisotropy pattern at the global scale.

On the other hand, theoretical studies have indicated that the BRDF, that quantifies the angular distribution of the reflected radiance, carries specific information on the landsurfaces (Asner, 2000) such as the spatial distribution

* Corresponding author.
E-mail address: cbacour@cea.fr (C. Bacour).

0034-4257/$ - see front matter © 2005 Elsevier Inc. All rights reserved.
doi:10.1016/j.rse.2005.06.008

of the scattering elements (Diner et al., 1999; Gao et al., 2003; Gerstl et al., 1986), *LAI*, *fAPAR*, fractional cover, clumping, or chlorophyll content (Bacour et al., 2002; Chen et al., 2003; Gemmell, 2000; Lacaze et al., 2002). Also, the reflectance directional signatures provide additional information to the spectral signatures to decouple the effects of biochemical and structural parameters. Integration of multi-angle observations is also maturing for improving characterization of surface roughness (Marticorena et al., 2004), landcover types (Bicheron et al., 1997; Lovell & Graetz, 2002; Zhang et al., 2002) and heterogeneity (Pinty et al., 2002). Nevertheless, whether they concern quantitative (biophysical variable estimation) or qualitative (land cover classification) characterizations of the Earth surface, most of these studies use the directional information to supplement the spectral dimension of the measurements. It is not clear whether there is a specific information provided by the directional signature.

Still, the angular variability of vegetation and soil reflectance has long been investigated with radiative transfer models, supported by field-based (Deering & Leone, 1986; Kimes, 1983; Kriebel, 1977; Sandmeier, 1999) and laboratory measurements (Briottet et al., 2004; Liang et al., 1997; Solheim et al., 2000). More recently, airborne sensing data (Camacho de Coca et al., 2004; Leroy & Bréon, 1996; Tsay et al., 1998) have provided a larger – but still limited – sample of directional signatures. Complementarily to samples of reflectance directional signatures gained by temporal compositing over short time periods of single-angle images acquired by AVHRR or MODIS (MODerate resolution Imaging Spectrometer), complete samples of land surface BRDFs are provided by spaceborne measurements of POLDER (POLarisation and Directionality of the Earth's Reflectance; Bicheron & Leroy, 2000; Deschamps et al., 1994) and MISR (Multiangle Imaging SpectroRadiometer; Diner et al., 1999), that measure near – simultaneously the reflectance of a given Earth target from various viewing directions.

The present study analyzes the unrivaled database of BRDF measurements acquired by the POLDER spaceborne instrument. The analysis of the variability of the directional signature as a function of the vegetation coverage is undertaken to assess whether the BRDF can be interpreted as a specific signature of the underlying surface. The data analysis is made possible by reducing the BRDF dimensionality with a kernel-driven radiative transfer model. Finally, we investigate the possibility of using a biome dependent directional model to normalize reflectance measurements.

2. Materials and methods

2.1. POLDER reflectance database

The reflectance data were acquired during the 8 months of the POLDER-1 mission. A single path provides up to 14 measurements, acquired at a spatial resolution of about 6 km, from various directions with view zenith angles up to 70°. Although POLDER provides measurements in 8 spectral bands, we mostly analyze here those at 670 and 865 nm representative of the red and near IR. The measurements have been geo-coded, calibrated, cloud screened and partially corrected for atmospheric transmission and scattering (Bréon & Colzy, 1999; Hautecoeur & Leroy, 1998; Leroy et al., 1997). The cloud screening relies on three tests using (1) derivation of the pressure of the main reflectors (surface or clouds) based on the ratio of the channels at 763 and 765 nm in the oxygen absorption band, (2) polarized reflectance that exhibits very specific values for liquid phase clouds at scattering angles close to 140°, (3) a spatially variable threshold on the 443 nm reflectance and its angular variation. Cloud free pixels are then corrected from absorbing gases (O_3, O_2, and H_2O) and stratospheric aerosols. Oxygen and water vapor amounts are derived from a differential absorption technique using, respectively the measurements at 763 and 765 nm, and at 865 and 910 nm; the ozone correction uses TOMS/ADEOS data. For the data used in this paper, there is no correction for tropospheric aerosols.

A monthly composite of the various satellite overpasses provides a very dense sampling of the BRDF for view angles up to 70°, with small variations of the sun angle (roughly 10°). For natural targets, the BRDF is not a measurable quantity stricto sensu as it requires perfectly collimated beams of illumination and observation, while the sunlight is partly diffuse and the measurements involve conical geometries. Satellite measurements therefore provide an approximation of the BRDF, from few observation geometries. The BRDF error increases with atmospheric scattering (i.e. more diffuse radiation) so that significant aerosol load must be avoided. Besides, the approximation is better justified in the near IR than in the visible as the scattering optical thickness is then smaller. Although our satellite measurements do not provide a sampling of the BRDF per se, we use this terminology in the following as it is widely used for similar applications.

The POLDER dataset of this study expands an earlier version discussed in (Bicheron & Leroy, 2000): 22989 different sites were selected to sample the Earth biomes based on criteria regarding to the quality of measurements (smooth variability over the acquisition period) and their directional coverage (uniform distribution over the hemisphere). Significant aerosol loads have a strong impact on the lower wavelength measurements (443 and 565 nm in particular). Because of the variability of the aerosol load, targets that are affected by aerosol events show a noisy directional diagram (based on more than 10 different satellite overpasses). They are removed from the further analysis based on the smoothness threshold on the observed directional signatures, which significantly lessens the aerosol impact in our results. There is nevertheless some remaining aerosol contamination in the database, which is

expected to be more significant in the visible channels than in the near infrared. Another source of noise in the data is the evolution of the targets during the period of synthesis. The database was processed and made available by Medias France (Lacaze, 2003).

2.2. Semi-empirical BRDF model

The large number of directional measurements available for each site, with a large range of illumination geometries, precludes an easy quantitative interpretation of the informational content of the directional signatures. The directional reflectance measurements for each spectral band were therefore fitted by a three-parameter semi-empirical model (Maignan et al., 2004):

$$R(\theta_s, \theta_v, \phi) = k_0 + k_1 \cdot F_1(\theta_s, \theta_v, \phi) + k_2 \cdot F_2(\theta_s, \theta_v, \phi) \quad (1)$$

The F_i functions, also referred to as kernels, model theoretical directional signatures $R(\theta_s, \theta_v, \phi)$ in the ad hoc observation geometries (defined by the solar zenith θ_s, view zenith θ_v, and relative azimuth ϕ, angles). Their relative contribution to the observed reflectance is weighted by the corresponding k_i parameter to estimate. k_0 corresponds to the isotropic contribution of the surface, and may include the contribution from multiple scattering, which is more isotropic than the single scattered one.

The F_1 kernel is based on the analytical representation, according to geometric optic considerations, of the reflectance by a flat Lambertian surface covered with randomly distributed spheroids having the same optical properties as the soil (Lucht et al., 2000); it is often referred to as the *geometric* kernel. F_1 is typically bell-shaped (higher nadir reflectance compared to off-nadir in the perpendicular plane of observation, i.e. for relative azimuth angle of 90° and 270°). In the principal plane, the reflectance increases smoothly from oblique directions to backscattering (Fig. 1a). The F_2 kernel models the reflectance of a theoretical turbid vegetation canopy with high leaf density in the single scattering approximation; it is also referred to as the *volumetric* kernel. The original formulation (Ross, 1981) was modified to account for the hot spot effect within turbid media (Maignan et al., 2004). The directional shape of F_2 resembles an upturned bowl in the perpendicular plane. In the principal plane, the F_2 kernel shows a strong and narrow reflectance increase towards backscattering (Fig. 1b). The hot spot half width parameter was fixed here to 1.5°, corresponding to the mean value estimated for most of the Earth's targets, because of its little variability at the global scale (Bréon et al., 2002). Note that this should have only a marginal impact on the retrieved values of the model parameters as the hot spot directions are rarely sampled in the BRDF database.

Although the F_1 and F_2 functions are based on physical considerations, they are strong approximations in the radiative modelling. Besides, there is no justification for the linear compositing of the two functions, in particular in the case of a thin vegetation canopy overlying a rough surface. Thus, one should refrain from too much physical interpretations of the k_i inverted parameters. Nevertheless, this very simple model has shown a surprising capability at reproducing the measured directional signatures of the main landsurfaces (with the exception of ice and snow covers) with high accuracy (Maignan et al., 2004), significantly better than several others analytical models. In fact, the measurement-fit difference (typically of the order of 0.01 or less) has a noise-like directional pattern: it does not show any specific pattern indicating the inadequacy of the model to reproduce the measurements under particular observation geometries. Thus, we argue that the three parameters contain most of the reflectance directional information for view angles of less than 60°, i.e. those accessible to most Earth remote sensing instruments.

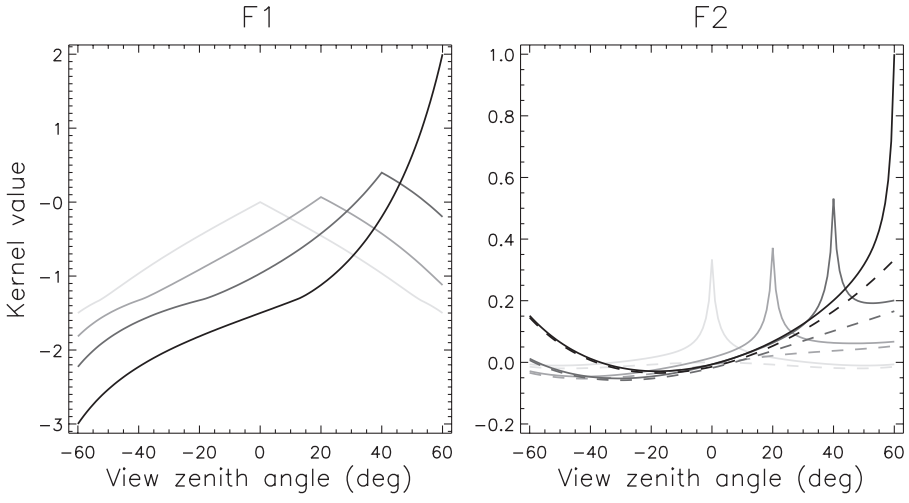

Fig. 1. Values of the F_1 and F_2 kernels in the principal plane, for four values of the solar zenith angle (0°, 20°, 40° and 60°). Darkening lines correspond to increasing θ_s values. The new implementation of the F_2 kernel (solid lines) accounting for the hot spot effect is compared to the original one (dashed lines).

Table 1
Distribution of the selected sites within the seven biome classes

	Grasses and cereal crops	Shrubs	Broadleaf crops	Savannas	Broadleaf forests	Needleleaf forests	Unvegetated areas	Total
Number of sites	676	1362	139	497	190	114	533	3511
Percentage	19.2%	38.8%	3.9%	14.2%	5.4%	3.3%	15.2%	100%

2.3. Data processing

From the original BRDF database, we selected targets with more than 120 observations in each spectral bands to ensure reliable estimates, and retained only those with a view angle of 60° or less, because more oblique views are increasingly affected by atmospheric scattering. The reflectance model was inverted against the measurements using a standard least square procedure. Any variation of the target reflectance within the one-month period of synthesis is not explicitly accounted for. Such variation, together with cloud contamination and atmospheric effects not properly corrected for, results in noise in the data that cannot be reproduced by the BRDF model. Thus, the targets with a measurement-model correlation coefficient less than 0.75 at 670 nm or 0.85 at 865 nm were discarded. The signal to noise is generally lower in the visible due to a combination of lower surface reflectances and larger atmospheric effects.

For further analysis, a vegetation class was assigned to the targets. The classification is based on MODIS results that partitions land surfaces into 7 biome types at a spatial resolution of 1 km (Knyazikhin et al., 1999; Zhang et al., 2002): (1) grasses and cereal crops, (2) shrubs, (3) broadleaf crops, (4) savannas, (5) broadleaf forests, (6) needleleaf forests, (7) unvegetated areas—deserts. An 11×11 km^2 (or 121 pixels) region centered on the POLDER targets (of nominal size 6×6 km^2) was used to identify the dominant biome and the spatial variability. Only those targets that show a dominant cover (i.e. more than 80% fractional cover) are kept for further analysis so as to ensure a thematic homogeneity and to prevent potential misclassification problems. Note that a fractional cover of 80% roughly corresponds to 97 pixels among 121 that are affixed the same biome type. In addition, snow covered pixels, identified by a somewhat larger reflectance in the visible than in the near IR and leading to high measurement-fit differences, were rejected.

After this stringent quality control procedure, 3511 out of 22989 sites are kept for further analysis, the distribution of which is given in Table 1.

3. Analysis of the directional signature variability

3.1. Examples of biome BRDFs

Fig. 2 shows directional measurements, in the principal plane, of a few selected targets representative of the 7 biome types. The remarkable quality of the fit by the semi-empirical model is typical of the results obtained on the whole of the dataset. The BRDF samples appear fairly similar between the biomes. The main noticeable differences reside in the spectral dimension of reflectance, i.e. relate to the differences between the reflectance levels measured in the four wavelengths. Accordingly, the "deserts" class is typical of soil backgrounds with similar reflectance levels in the red and near infrared. Conversely, "broadleaf forests" and "needleleaf forests", and in some extent "savannas", present an important gap of their optical properties between the visible and near infrared domains, as expected for dense vegetation covers. The "grasses and cereal crops", "shrubs", and "broadleaf crops" sites, rather correspond to sparse vegetated areas, intermediate between the two former cases.

In the following, the study is restricted to the red (670 nm) and near infrared (865 nm) domains commonly used to characterize vegetation covers through the use of NDVI.

3.2. Distribution of the estimated parameters

The distribution characteristics of the retrieved k_i parameters at 670 and 865 nm are given in Table 2 and Fig. 3. Their shape and the corresponding extremum values agree with those found for the coefficients of the Roujean model, inverted from POLDER measurements over Australia (Lovell & Graetz, 2002). The wider distribution observed for k_0 in the red than in the near infrared traduces the higher variability of the reflectance measurements because of the larger contrast between the optical properties of absorbing leaves and soils. k_2 values are generally larger in the near infrared than in the visible, while they are of similar magnitude for k_1 in the two wavebands. k_2 plays the role of the leaf reflectance in the radiative transfer formulation; its spectral dependency can be interpreted by the increase of radiation scattering by leaf layers from red to near infrared due to the vanishing of absorption by chlorophylls. In the following, k_1 and k_2 inverted for each site and normalized by k_0 are used to quantify the directional variation of the reflectance, with respect to the isotropic component, and are therefore considered as the directional parameters:

$$R(\theta_s, \theta_v, \phi) = k_0 \left[1 + \frac{k_1}{k_0} \cdot F_1(\theta_s, \theta_v, \phi) + \frac{k_2}{k_0} \cdot F_2(\theta_s, \theta_v, \phi) \right] \quad (2)$$

In order to assess for the robustness of the estimates, we analyzed 503 sites (out of 3511) that were sampled at

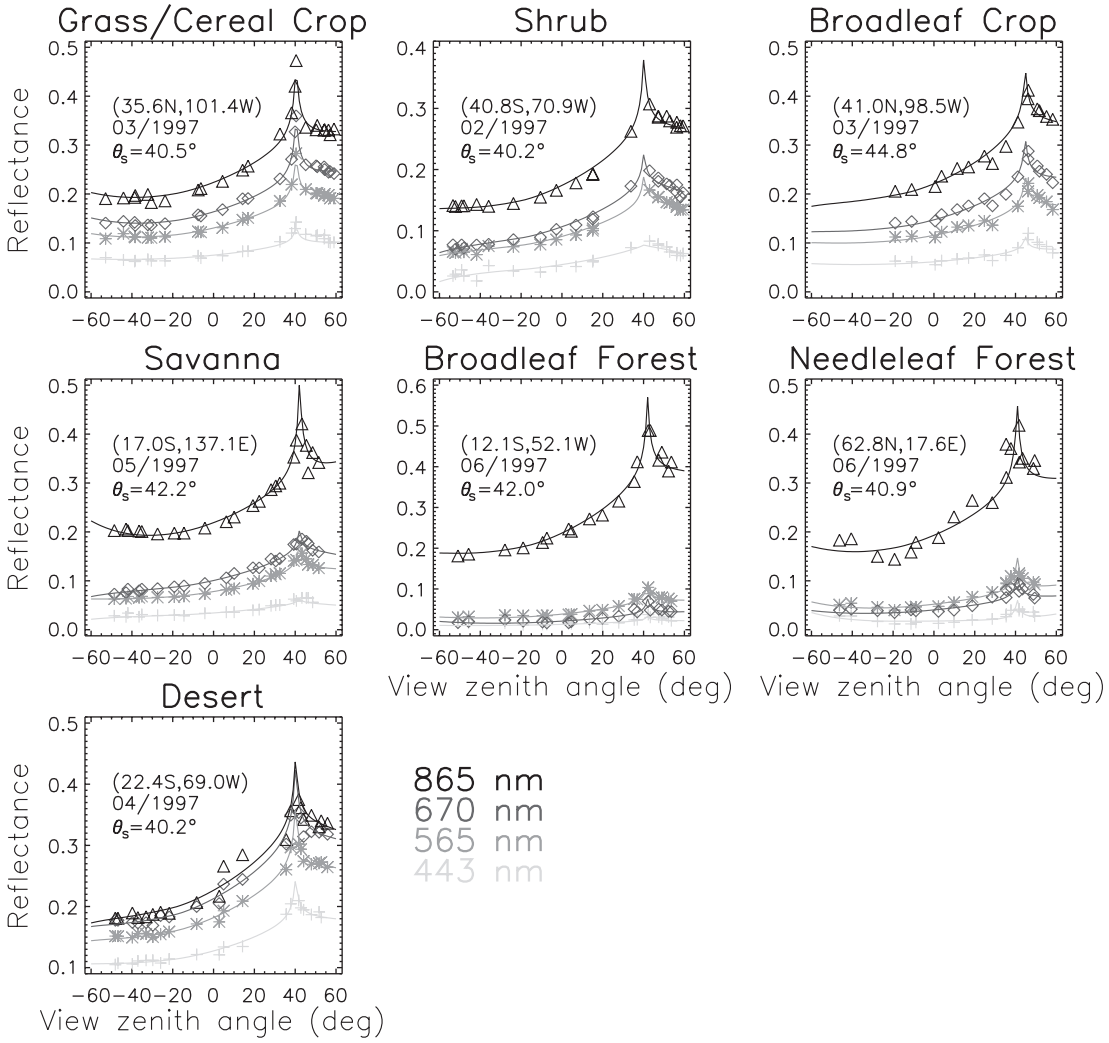

Fig. 2. Representative bidirectional reflectance signatures of the seven biome types in the principal plane at 443, 565, 670 and 865 nm, for a solar zenith angle close to 42°. The lines show the model BRDF after inversion of its parameters using all reflectance measurements. The symbols represent the error of fit to the measurements acquired around the principal plane (±5°), plus the corresponding reflectances simulated in the principal plane.

different months. The temporal variation of the retrieved parameters is shown in Fig. 4 where, for each site, the parameters estimated at a given acquisition period are plotted against the values retrieved at another one. For each case, the root mean square error and correlation coefficient quantify the dispersion of the estimates around the one-to-one line. This dispersion is due to structural changes of the corresponding surfaces during the vegetative cycle together with uncertainties in the estimates resulting both from the measurement errors and the inadequacy of the model to reproduce reality. The isotropic parameter – k_0 – appears to be the most robust and stable in time. The higher variance found for k_1/k_0 and k_2/k_0 can be related to an higher sensitivity to temporal variations both in leaf amount and sun zenith angle, but also to estimation instabilities because of compensation effects between the kernels (Gao et al., 2003; Lovell & Graetz, 2002).

Indeed, k_1 and k_2 have been reported to be not strictly independent of one another because the corresponding functions F_1 and F_2 are somewhat correlated. This may explain the few negative values obtained for the directional parameters k_1/k_0 and k_2/k_0. They may also arise from reflective properties of the observed surface not accounted for by the simple physics of the model. Negative k_2 values translate to the total BRDF by an "anti-hot spot" effect, i.e. a sharp decrease of the reflectance in the retro-solar direction. This occurs when no measurements are available around backscattering to constrain the model inversion. They concern only 4% and less than 0.1% of the sites (out

Table 2
Statistics on the estimated values of the Ross–Li model parameters at 670 and 865 nm: minimum, mean (in italic), standard deviation (in brackets), and maximum, values

	670 nm	865 nm
k_0	0.003 *0.159* (0.082) 0.450	0.128 *0.264* (0.060) 0.499
k_1	−0.058 *0.023* (0.018) 0.099	−0.062 *0.027* (0.022) 0.135
k_2	−0.297 *0.152* (0.101) 0.633	−0.063 *0.363* (0.135) 1.040

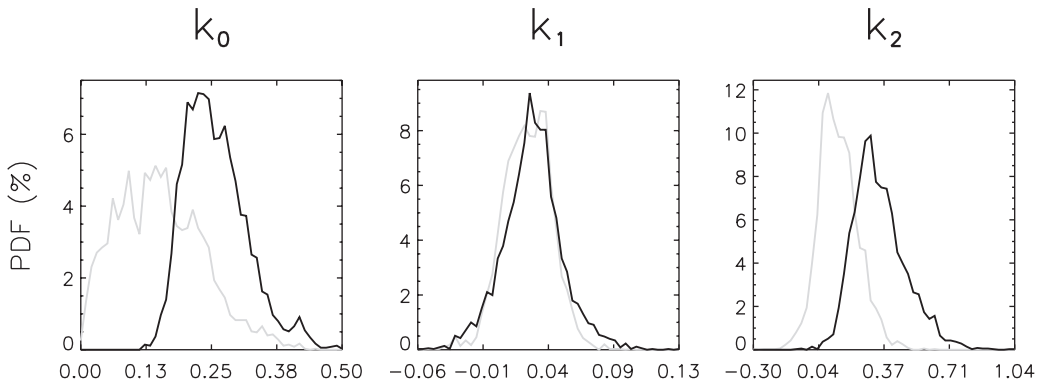

Fig. 3. Histograms of the model parameter estimates (probability density functions in percentage for ranges of variation of the parameter values discretized into 50 bins) at 670 (gray) and 865 (black) nm.

of 3511) at 670 and 865 nm, respectively. Negative k_1 values do not impact the BRDF in such a manifest manner; 10% of the sites are concerned at both wavelength. We chose to keep the corresponding sites in the following because the negative parameters, even if considered as nonphysical, do not affect the quality of fit in the directions of observation and will impact insignificantly the analysis. Moreover neither dependency with the biome type nor potential contamination by snow or cloud was detected.

The temporal stability of the k_0 estimates suggests a limited variation of the surface reflectance. We have thus postulated that the higher dispersion around the one-to-one line for the directional parameters (Fig. 4) is the result of instabilities in the inversion due to correlations between F_1 and F_2. Consequently, we have investigated the potentiality of determining a more robust directional parameter for characterizing the surface anisotropy, which reduces the compensations between k_1/k_0 and k_2/k_0. It is defined as a linear combination of these, of the form $(k_1+\alpha*k_2)/k_0$. The empirical α coefficient is tuned so as to maximize the correlation between the values estimated at different acquisition periods. With α varying between -1 and 1,

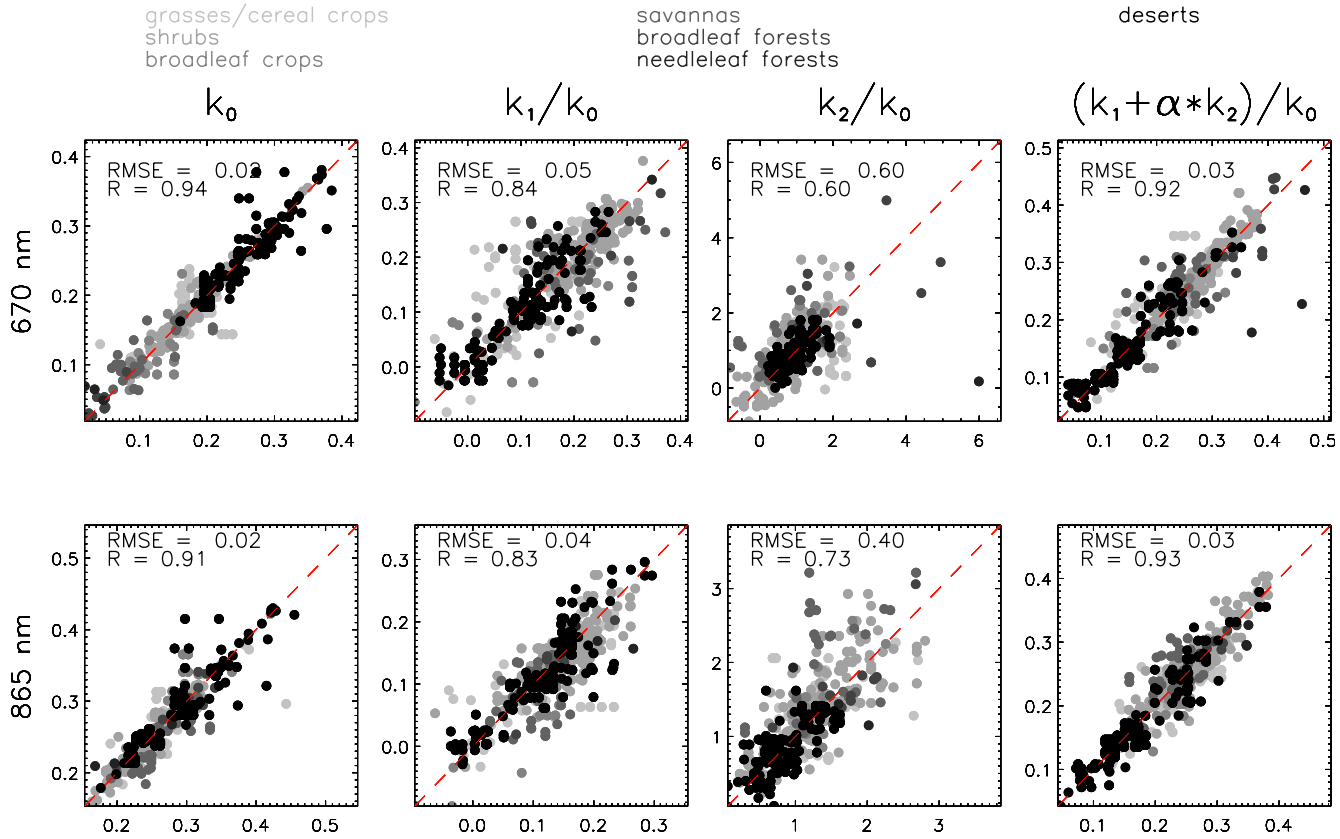

Fig. 4. Scatterplots of the parameter estimates for the sites sampled during different time intervals. For each case, the root mean square error (RMSE) and correlation coefficient (R) are shown. $\alpha=0.066$ at 670 nm and $\alpha=0.088$ at 865 nm.

the variation intervals of the correlation coefficient range from [0.60; 0.92] in the red and [0.69; 0.93] in the near IR, the maximum being reached for α of 0.066 and 0.088, respectively. This way, the correlation coefficients for this novel directional parameter are similar to those found for k_0 in both wavelengths. This finding clearly demonstrates that correlations between F_1 and F_2 leads to some noise in k_1 and k_2 retrieval, that can be reduced by use of a linear combination between the two parameters. In the following, its relevance is evaluated for discriminating the biomes on the basis of their directional signatures.

The relation of the k_i coefficients with the biome type is examined in Fig. 5. The dependency of k_0 with the biome type is consistent with previous observations (Leroy & Roujean, 1994) according to which that coefficient represents the physical evolution of the surface. The inter-class variability is larger in the red, and is coherent with the expected relative proportion of leaves per biome, considering the contrast between the optical properties of leaves and soils. For dense canopies (broadleaf and needleleaf forests), the range of variation is narrow around a low mean value, traducing high absorption of the incident radiation by a large amount of green leaves. For sparser canopies, the minimum value of the variation interval changes only slightly while the maximum value (and consequently the spectrum of k_0 values) increases, together with the contribution of the background to the reflectance. Savannas and broadleaf crops in one hand, and grasses and cereal crops and shrubs in another hand, exhibit similar features. Such broad ranges of variation reveal very different vegetation situations and growth stages within a given biome type. The unvegetated class stands apart with higher values of the isotropic component due to higher reflectance values for soils in the red. The differences between the ranges of variation of k_0 are smoothed out in the near infrared. This is likely due to the reduced contrast between the optical properties of soil background and leaf layers, and to higher contribution of the multiple scattering, more isotropic than the single scattered radiation. Needleleaf forests are however an exception with a narrow range of lower k_0 values. This result agrees with the lower reflectances observed for needle leaves that, combined to a high clumpiness, translate to increased absorption efficiencies at the canopy level in the near IR (Rock et al., 1994; Williams, 1991). The higher variability of the k_0 values within the classes than between them precludes the discrimination of the different vegetation types on that basis alone.

Inspection of the directional coefficients does not enlighten much on that aspect as, for most cases, they also present a variability intra-class superior to that inter-class at both wavelengths. Broadleaf and needleleaf forests however depart with globally higher range of variation of k_2/k_0 at 670 nm and of the k_1/k_0 parameter. The lowest values of k_2/k_0 in the red are obtained for shrublands and deserts (unvegetated class) where the vegetation cover is sparse. $(k_1+\alpha*k_2)/k_0$ exhibit globally larger mean values for forests, while deserts present the largest range of variation in the near infrared, spanning from zero up to a maximum value close to that of forests.

Because F_1 and F_2 have similar directional behaviour with however different range of variations, the sole analysis of the joint values of k_1/k_0 and k_2/k_0 does not enable to determine which of the scattering (surface-geometric or volumetric) regime dominates. This can however be appraised regarding to the shape of the BRDF in the perpendicular plane of observation, because bell-shaped

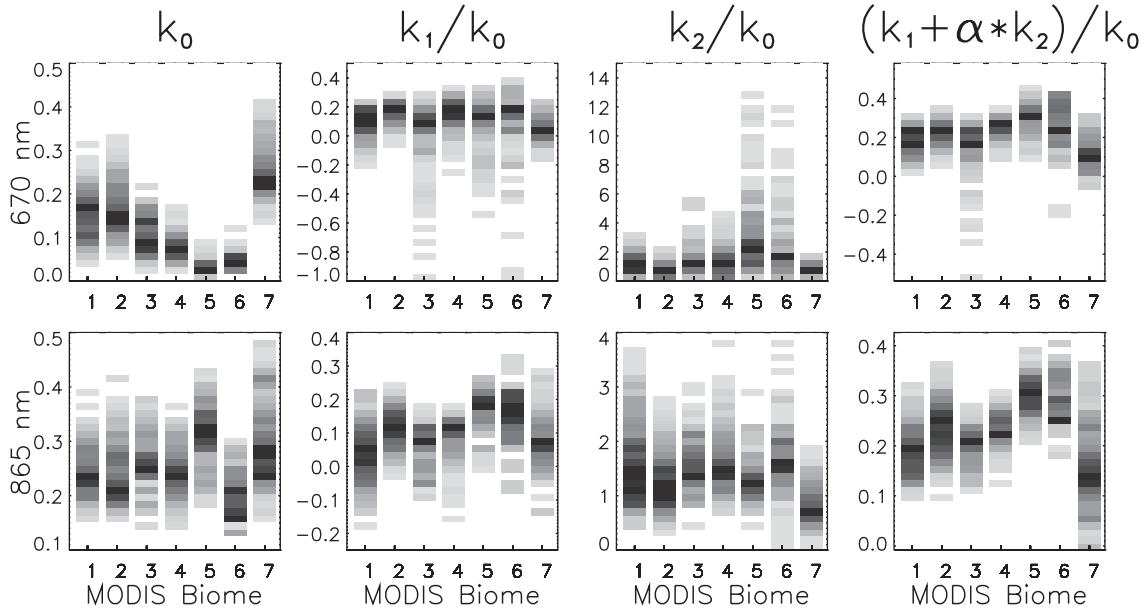

Fig. 5. Density of the k_i estimates within their range of variation as a function of the biome type, in the red and near infrared. The biomes considered are: (1) grasses and cereal crops, (2) shrubs, (3) broadleaf crops, (4) savannas, (5) broadleaf forests, (6) needleleaf forests, and (7) deserts. Each bar corresponds to an histogram where cells darkens with the population density. Extreme values of k_1/k_0 and k_2/k_0 that are underrepresented were discarded to increase readability.

BRDFs are determined by prevailing surface-scattering effects (F_1 function, see Fig. 1) while F_2 predicts directional reflectance variations of the form of an upturned bowl. The ratio of the nadir reflectance to that simulated at $\theta_v=60°$ in the perpendicular plane and for an average solar zenith angle of 40°, ρ_{60}/ρ_0, is used to quantify the origin of the anisotropy: $\rho_{60}/\rho_0<0.95$ (conversely, $\rho_{60}/\rho_0>1.05$) corresponds to bell-shaped (bowl-shaped) anisotropy patterns. The proportion of "bell-shaped" sites (51%) comes out to be larger than that of bowl-shaped ones (15%) in the red. This difference is reduced in the near infrared where 19% of the sites are bell-shaped and 22% are bowl-shaped. The dispersion of the ρ_{60}/ρ_0 values was similar to that found for the directional parameters and does not allow to discriminate between different vegetation types. The results do not allow to confirm the hypothesis that bowl- and bell-shaped anisotropy patterns in the red are signatures of the surface heterogeneity (Pinty et al., 2002). According to this theory, homogeneous surfaces, either plant canopies or bare soils, lead to mostly bowl-shaped BRDFs, while bell-shaped BRDFs tend to occur for heterogeneous landscapes. The important proportion of bell-shapes situations at the coarse spatial resolution of POLDER seems to indicate that the bowl-shape vs. bell-shape anisotropy feature is not a reliable information to detect surface heterogeneity. As a matter of fact, at such spatial resolution, the targets are expected to be more thematically homogeneous than at finer scales (Garrigues et al., submitted for publication; Pinty et al., 2002).

3.3. Biome discernability

The biome discernability is examined in Fig. 6 (top) with respect to the spectral dependency of the retrieved parameters. The contour plots represent the convex hulls of the density distributions that encompasses 68% of the data; they correspond to those departing from the mean from, at the maximum, the value of one Gaussian standard deviation.

The contour plot of k_0(670 nm) versus k_0(865 nm) resembles a typical red against near infrared reflectance diagram commonly used in remote sensing to discriminate vegetation covers from bare soils. Because the differences in reflectance levels between these two wavelengths essentially relates to the leaf optical properties and their amount, the location of a point in this bidimensional spectral space therefore informs on the amount of photosynthetically active vegetation. Consequently, the biomes corresponding to the denser vegetation types, broadleaf and needleleaf forests, appear distinctly on the left of the diagram while the unvegetated sites scatter along the one to one line. The other biomes are distributed in between these extreme cases – the sparser the vegetation is, the closer to the soil line it gets – with a noticeable overlapping of the convex hulls. The spectral hulls of the various biome types are not sufficiently distinct from one another – even though they are corrected from the directional effects – to identify them accurately on that basis alone. We here confirm the results of previous studies (Zhang et al., 2002). Unfortunately, it appears that the directional information (the normalized k_1 and k_2

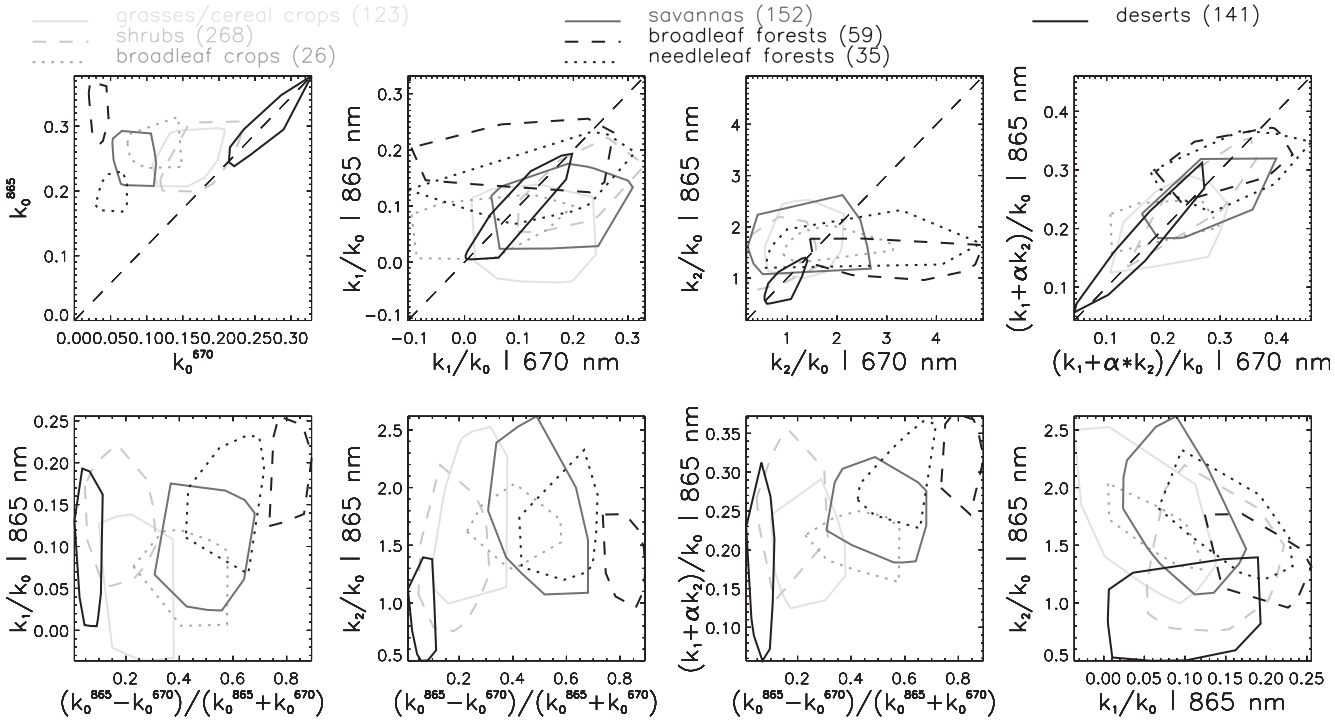

Fig. 6. Convex hulls of the density distributions of the parameters values for each biome type. Top: Comparison between the values estimated at 670 and 865 nm. Bottom: Relation between the different parameters at 865 nm. Each contour encompasses 68% of the most probable estimated values for a given biome. The number of sites used to build the convex hulls are given in brackets.

coefficients) is not more valuable as the confusion between hulls is even larger. The observed dispersion of the hulls enforced the previous results of Fig. 5. The unvegetated class stands aside with values of k_1/k_0 and k_2/k_0 highly correlated between 670 and 865 nm (with correlation coefficients, respectively of 0.96 and 0.86), because of similar optical properties at both wavelengths. Estimation errors or compensation effects between the kernels alone cannot explain such important overlapping of the convex hulls. Indeed, the use of the linear combination between k_1/k_0 and k_2/k_0 (which was shown to be more robust) produces a large overlapping. $(k_1+\alpha*k_2)/k_0$ presents a rather weak spectral dependency. This may indicate that that observed for k_1/k_0 and k_2/k_0 taken individually (Fig. 6) is mainly an artifact resulting from the above mentioned compensation errors.

The relations between the spectral and directional parameters are shown in Fig. 6 (bottom). The spectral information is here reduced to the normalized difference between $k_0(865)$ and $k_0(670)$, $(k_0^{865}-k_0^{670})/(k_0^{865}+k_0^{670})$. Again, it appears that the respective signature of the biomes is better discriminated in the spectral space than based on the directional dimension.

The perusal of the convex hulls in the bidimensional parameter spaces reveals only slight discernability between the 7 biomes considered in this study. A more quantitative analysis was performed by means of a simple classification algorithm in order to partition the data space into seven clusters of similar characteristics (routine CLUSTER of the Interactive Data Language). Two cases were considered (Table 3): accounting for the spectral information only and for the directional information in the near infrared only.

The classification based on the normalized reflectance estimated in the red and near infrared recognizes satisfactorily the predefined forest biomes (Table 3 top): for each, the whole of the corresponding sites are affixed to a single class (E1 and F1). This confirms that, except little contamination from other biomes, broadleaf and needleaf forests have very specific spectral properties. Similarly, 86% of the deserts is well-identified (classes A1 and B1). Grasses/cereal crops and shrublands on the one hand, and broadleaf crops and savannas on the other hand, appear to have similar spectral features. Thus, the classification performed on the basis of the spectral information alone separates the data space into 5 classes of similar red-near infrared signatures. The consistency with the original MODIS biome classification is not surprising as its definition principally relies on the spectral information; part of the discrepancies are explained by the accounting for the temporal evolution of the spectral properties of the sites in the MODIS classification.

Table 3
Results of the classification exercise accounting for (a) the spectral information only (top), (b) the directional information only (bottom)

Information	Classes	Biomes						
		1	2	3	4	5	6	7
k_0^{670} k_0^{865}	A1	0	0	0	0	0	0	37
	B1	5	17	0	0	0	0	49
	C1	43	29	6	0	0	0	14
	D1	48	53	7	2	0	0	0
	E1	0	0	6	2	100	0	0
	F1	0	1	0	18	0	100	0
	G1	4	0	81	78	0	0	0
k_1^{865}/k_0^{865} k_2^{865}/k_0^{865}	A2	3	1	0	0	0	0	55
	B2	0	20	0	1	2	0	35
	C2	0	27	0	4	84	55	2
	D2	37	0	23	4	0	0	1
	E2	24	0	6	10	0	0	0
	F2	17	19	45	50	13	40	0
	G2	19	33	26	31	1	5	7

Per biome type, the percentage of sites affixed to each class is given, such that the column sum is equal to 100%. The biomes considered are: (1) grasses and cereal crops, (2) shrubs, (3) broadleaf crops, (4) savannas, (5) broadleaf forests, (6) needleleaf forests, and (7) deserts.

The classification based on the directional parameters in the near infrared results in an higher repartition of the sites within each of the seven classes (Table 3 bottom). Deserts appear better defined in this bidimensional space than the other biomes, as two classes (A2 and B2) encompasses 90% of the corresponding sites. They are mixed with few shrubland sites (21%), where the sparseness favors the influence of the background. Most of the broadleaf (84%) and needleleaf (55%) targets are also included within a same class (C2), together with some of the shrublands. 61% of the sites corresponding to grasses and cereal crops are grouped in two classes (D2 and E2), with about a quarter of the broadleaf crop sites and some savannas. The two last classes (F2 and G2) mix most of the sites corresponding to grasses/cereal and broadleaf crops, shrubs, savannas, and about half of the needleleaf forests.

As a conclusion, the statistical analysis show no clear distinction between different vegetation types regarding to their reflectance directional signatures.

3.4. Variability of the directional signatures with the biome

That variability of measured BRDFs is further investigated with respect to predefined bidirectional anisotropy pattern types, representative of the main directional signatures. Considering the bidimensional space defined by the values of k_1/k_0 and k_2/k_0, and for a given number of classes, the automatic classification identifies the regions of the most similar directional features. Each cluster is assigned a Bidirectional Anisotropy Standard shapE (BASE). It consists in a directional model depending on only one multiplicative parameter $\tilde{k}_0$:

$$R(\theta_s,\theta_v,\phi) = \tilde{k}_0\left[1+\frac{k_1}{k_0}\bigg|_{\text{class}}\cdot F_1(\theta_s,\theta_v,\phi)+\frac{k_2}{k_0}\bigg|_{\text{class}}\cdot F_2(\theta_s,\theta_v,\phi)\right] \quad (3)$$

$\tilde{k}_0$ is adjusted from the reflectance measurements according to a standard least square method, while the $(k_1/k_0, k_2/k_0)$

values correspond to the barycenter of the class considered. Each site is then assigned the BASE type that minimizes the RMSE between the measurements and the adjusted model. For an increasing number of BASE classes, the variation of the RMSE of fit to the actual measurements provides a new insight on the variability of the biome anisotropic features (Fig. 7).

In the red, 3 BASEs suffice to represent the variability of the observed anisotropy for the vegetation biomes, when 6 classes are required for deserts. These subjective numbers correspond to the minimum number of BASEs beyond which the RMSE of the fit does not decrease significantly. The differences between deserts and the other vegetation biomes derive firstly from the higher reflectance levels in the red associated to unvegetated areas. Most of all, this indicates a wider variability of the directional signatures for deserts than for vegetated surfaces. The order of magnitude of the RMSE is similar at both wavelengths in spite of the different reflectance levels. The higher signal to noise ratio of the measurements in the near infrared translates to an increased quality of the fit, which in return enhances the dissimilarity of the main anisotropic features as attested by the larger number of BASE classes (7 up to 10) required to reproduce the variability of the measurements. Conversely, the low reflectances measured in the red are more subject to noise, which hampers to properly discriminate between two different BRDFs; the anisotropic features between biomes are consequently smoothed out.

3.5. Discussion

For the sake of clarity, we have only presented the results of the Ross–Li model even though other linear kernel-driven models were applied the same way on the POLDER dataset. The Roujean (Roujean et al., 1992) and RossThick–LiDense Reciprocal (Wanner et al., 1995), differing by their description of the structural attributes of the scattering medium, provided very similar results in terms of variability of the parameter estimates with the biome type. The variability of the directional parameters with the biome type expresses the diversity in structural situations following the vegetative cycle within a given biome class. These findings indicate the inadequacy of the biome classification to capture the actual vegetation structural state and phenology.

Residual aerosol effects that have not been properly filtered by the selection procedures are a source of uncertainty in the estimation of the directional parameters. Nevertheless, most of the analysis on the variability of the directional signatures with biome type relies on the measurements at 865 nm where the aerosol impact is small (small scattering optical thicknesses combined to high surface reflectances). Therefore we argue that unresolved aerosol effects, if any, have only a marginal impact on the previous findings.

The coarse spatial resolution of POLDER is another issue. One must question if the results obtained at 6 km are also valid at 1 km, the spatial scale at which the biome map classification is defined. Because radiance is additive, the BRDF of a mixed pixel is a linear combination of the

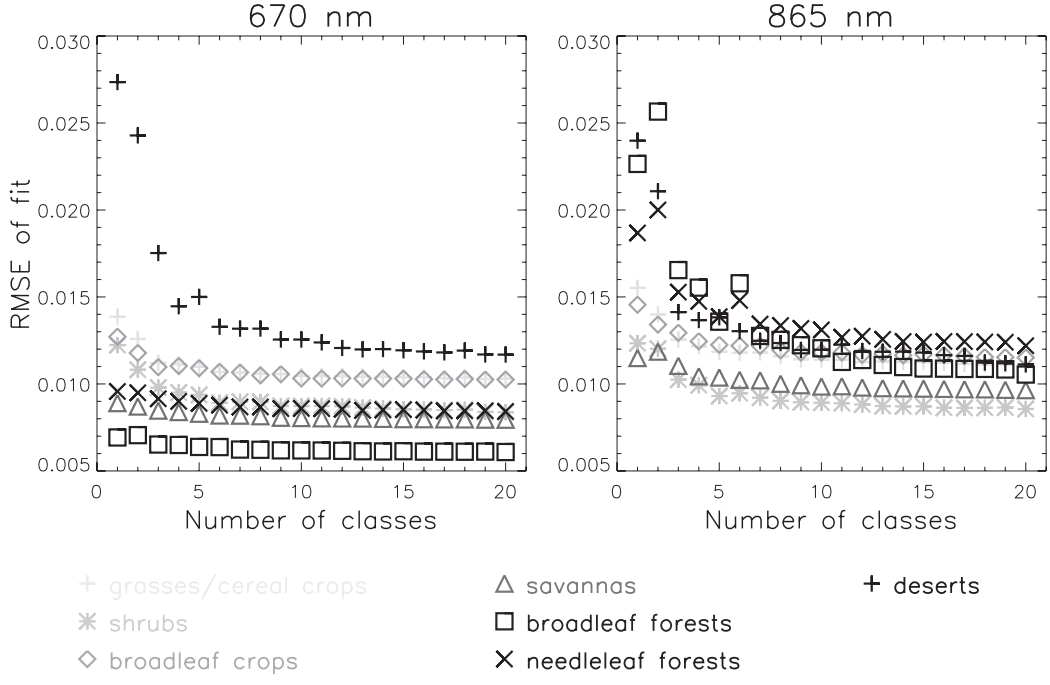

Fig. 7. Variation of the RMSE of fit with the number of BRDF classes considered at 670 and 865 nm, for (1) grasses and cereal crops, (2) shrubs, (3) broadleaf crops, (4) savannas, (5) broadleaf forests, (6) needleleaf forests, and (7) deserts. The RMSE corresponds to the average over all sites of each biome class.

directional signatures of the thematic surfaces it is made of. Consider a scene observed at a coarse spatial resolution; it is characterized by the surface parameters k_i^0(i=0,1,2). One can conceptually decompose that scene into an ensemble of homogeneous surfaces of corresponding parameters k_i^j. Then, according to Eq. (1), the k_i^0 are theoretically a linear combination of the k_i^j, weighted by the areal proportion of the different components (Roujean et al., 1992; Wanner et al., 1995). The issue of the spatial heterogeneity for the estimation (and interpretation) of the BRDF parameters therefore depends on the spatial scale at which that heterogeneity ceased to be detected. For most homogeneous and heterogenous landscapes, the degree of spatial heterogeneity (i.e. the variance of the radiometric signal) changes only slightly beyond 1-km resolution (Garrigues et al., submitted for publication). Therefore, one may reasonably assume that the results obtained at the coarse resolution of POLDER are also applicable at 1 km, the nominal spatial resolution of NOAA/AVHRR. Besides, the monitoring of vegetation dynamics from space is most often achieved with data at spatial resolutions similar to that used here (Lu et al., 2003; Maisongrande et al., 1995; McCloy & Lucht, 2004; Myneni et al., 1997; Running & Nemani, 1988) which makes this work very relevant. Finally, let us stress that the poor information content of directional signatures to discriminate land cover types has also been reported at finer resolution (Khlopenkov et al., 2004).

4. Global BRDF typology

An operational normalization of the bidirectional effects requires the a priori knowledge of the landsurface anisotropy (Cihlar et al., 1997; Csiszar et al., 2001). Indeed, the lack of a sufficient directional sampling hampers an accurate fit by classical semi-empirical models. We investigate here the possibility of using predefined BASE types for such reflectance normalization. Their justification follows the previous results according to which the Earth landsurfaces exhibit similar bidirectional reflectance shapes that mainly vary in magnitude.

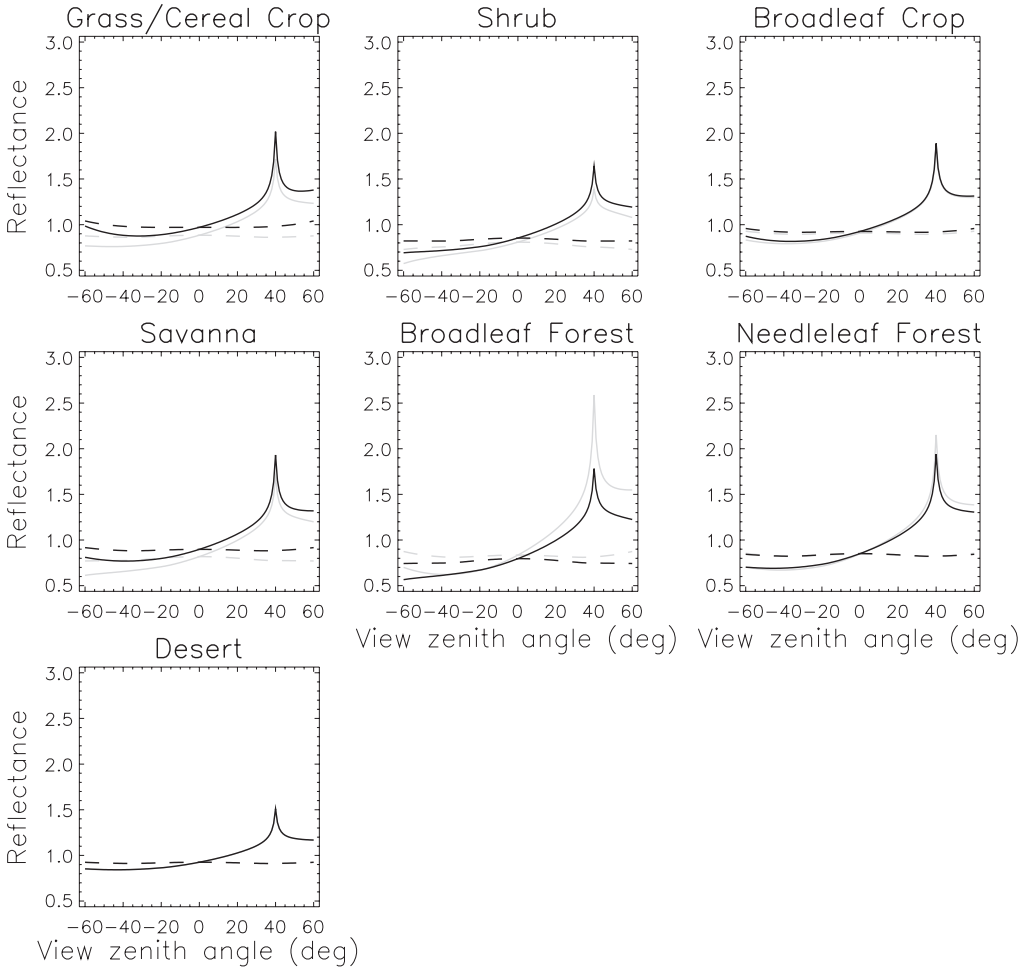

Fig. 8. Variation of the standard biome specific BASEs in the principal (solid lines) and perpendicular (dashed lines) planes, for a solar zenith angle of 40°, at 670 (gray) and 865 (black) nm.

4.1. Biome specific BASE types

In a similar way as in Section 3.4, each biome is assigned a bidirectional standard shape to characterize the anisotropy in the red and near infrared bands. They are now defined for each of the seven main vegetation covers as in Fig. 6 (i.e. the population of the directional parameters is restricted to the values within one standard deviation from the means):

$$R(\theta_s,\theta_v,\phi) = \tilde{k}_0\left[1+\frac{k_1}{k_0}\bigg|_{\text{biome}}\cdot F_1(\theta_s,\theta_v,\phi)+\frac{k_2}{k_0}\bigg|_{\text{biome}}\cdot F_2(\theta_s,\theta_v,\phi)\right] \quad (4)$$

The directional shapes of the biome specific BASEs are given in Fig. 8, in the principal and perpendicular planes and for a solar zenith angle of 40°; the corresponding coefficients k_1/k_0 and k_2/k_0 are provided in Table 4. For deserts, the BASEs are identical in the red and near infrared. This biome type, with shrubs in a lesser extent, shows the most isotropic behavior as expected. Before further investigating their potentials for normalization purposes, the ability of these BASE to fit actual measurements is evaluated.

4.2. Adequacy of the BASEs with the measurements

The inversion of a BASE against measured reflectance data requires a single free parameter, for each spectral band. To evaluate the ability of predefined BASEs to reproduce observed directional signatures, the corresponding RMS error of fit is compared to that obtained when all three k_i parameters of the Ross–Li model are let free. The results are gathered in Table 4 together with the characteristics of the biome specific BASEs. It also shows the median values of the estimated $\tilde{k}_0$ parameter for each biome, and the median values of the standard deviation of the observations σ (R_{obs}) which quantifies the amplitude of the directional signature. The statistical results provided were obtained both when using the full original POLDER database as well as the reduced one determined after stringent quality control.

Table 4
Directional parameters of the biome specific BASEs at 670 and 865 nm and reflectance measurement retrieval accuracy, for (1) grasses and cereal crops, (2) shrubs, (3) broadleaf crops, (4) savannas, (5) broadleaf forests, (6) needleleaf forests, and (7) deserts

	Biomes	number of sites	k_1/k_0	k_2/k_0	$\tilde{k}_0$	σ (R_{obs}) (×100)	RMSE (×100) biome BASEs	RMSE (×100) Ross–Li	EoN (×100) 1 BASE	EoN (×100) biome BASEs
670 nm	1	676	0.1112	1.2709	0.1583	2.45	1.18	0.98	1.32	1.22
		4462			*0.1309*	*2.52*	*1.34*	*1.11*	*1.46*	*1.42*
	2	1362	0.1945	0.5837	0.1627	2.69	1.01	0.74	1.27	1.07
		3874			*0.1526*	*2.63*	*1.21*	*0.91*	*1.38*	*1.30*
	3	139	0.0840	1.5642	0.1152	2.08	1.09	0.93	1.15	1.09
		1575			*0.1031*	*2.07*	*1.18*	*1.02*	*1.26*	*1.22*
	4	497	0.1800	1.1699	0.0782	1.69	0.84	0.74	0.90	0.91
		3300			*0.0784*	*1.76*	*1.02*	*0.92*	*1.07*	*1.12*
	5	190	0.1503	2.8778	0.0311	1.12	0.62	0.57	0.67	0.62
		2514			*0.0434*	*1.5*	*1.06*	*0.92*	*1.06*	*1.11*
	6	114	0.1444	2.0585	0.0501	1.52	0.9	0.81	0.92	0.90
		2749			*0.057*	*1.75*	*1.32*	*1.17*	*1.38*	*1.41*
	7	533	0.0724	0.8977	0.2584	2.98	1.40	0.93	2.30	1.45
		1341			*0.2544*	*3.04*	*1.63*	*1.04*	*2.37*	*1.73*
865 nm	1	676	0.0170	1.9043	0.2347	3.42	1.3	0.99	1.55	1.35
		4462			*0.234*	*4.19*	*1.75*	*1.20*	*1.81*	*1.84*
	2	1362	0.1441	1.0984	0.2555	3.9	1.13	0.74	1.19	1.19
		3874			*0.2583*	*4.05*	*1.34*	*0.89*	*1.38*	*1.43*
	3	139	0.0658	1.6257	0.2684	4.27	1.28	1.11	1.33	1.28
		1575			*0.2598*	*4.48*	*1.54*	*1.21*	*1.60*	*1.56*
	4	497	0.0941	1.6821	0.2455	4.33	1.02	0.86	1.10	1.09
		3300			*0.2475*	*4.42*	*1.35*	*1.07*	*1.39*	*1.39*
	5	190	0.2021	1.3195	0.3257	6.79	1.26	0.88	2.12	1.27
		2514			*0.2986*	*5.72*	*1.64*	*1.09*	*1.98*	*1.76*
	6	114	0.1426	1.6627	0.1913	4.27	1.47	1.01	1.78	1.42
		2749			*0.2204*	*4.46*	*1.99*	*1.35*	*2.21*	*2.18*
	7	533	0.0710	0.9056	0.2957	2.92	1.47	0.91	1.98	1.52
		1341			*0.2976*	*3.11*	*1.64*	*0.99*	*2.13*	*1.76*

The median values obtained for all sites of each biome are given for: the estimated $\tilde{k}_0$ parameter corresponding to the best fit of the biome specific BASEs to the measurements; the standard deviation of the measurements σ (R_{obs}); the RMSE of fit when considering the biome specific BASEs; the RMSE of fit when accounting for the three parameter Ross–Li model; the error of normalization (EoN) when considering only one BASE type; the error of normalization when using the adequate biome specific BASE types. For each biome, the first line corresponds to the results obtained on the same dataset used to determine the biome specific directional parameters; the second line (in italic) corresponds to the results obtained using all the sites of the POLDER archive.

The consistency between the two set of results indicates the fairly good generality of the biome specific BASEs, even though they are determined only from a limited number of sites. The root mean square errors of fit, in absolute values, are of the same order of magnitude at 670 and 865 nm because of the above mentioned lower signal to noise ratio in the visible. As expected, the error generally decreases inversely with the constraints imposed to the shape of the BRDF. This way, the full BRDF model (with three degrees of freedom) fits better the measurements than when the biome specific approach (1 degree of freedom per biome) is used. However, the differences in the RMS errors of fit between these interpolation approaches are generally slight, thus corroborating that a BASE captures satisfactorily the directional signatures of the corresponding biome type.

Fig. 9 shows the cumulative histograms of the RMSEs of fit for each biome, when considering the biome specific BASEs (left) and the three parameter BRDF model (right) at 670 and 865 nm. In the red, the higher errors observed for the desert sites is compatible with the previous result pointing out that more BRDF classes are required to reliably account for the directional variability for this biome. For vegetated surfaces, needleleaf forests corresponds to the predefined BASE with the worst fit to the observations. This is very likely due to lower signal to noise ratio, in relation to lower reflectance levels and consecutive increased atmospheric noise. Note that the high proportion of sites located in northern latitudes also enhances that latter issue as well as it can indicate residual snow contamination. The global adequacy of the adjusted biome specific BASEs with the measurements is in accordance with that found with more complex analytical models (Maignan et al., 2004). Considering the sites used for calibrating the BASE types, the median RMSE of fit is, respectively of 0.0123 and 0.0122 at 670 and 865 nm; it is of 0.0122 and 0.0159 when the whole of the sites are accounted for. The approach therefore ranks in between the performances of fit of the Walthall (RMSEs of 0.0133 and 0.0203 nm at 670 and 865 nm, respectively) and Roujean models (0.0116 and 0.0146). The error of fit is then, in relative units, of the order of 10% in the red and 5% in the near infrared.

4.3. Potentials of a BRDF typology for normalization issues

The benefit of using the predefined BASE biome types for normalization issues is now evaluated. The reflectance normalization is undertaken by simply multiplying a reflectance measurement by $BASE(\theta_s^0,0,0)/BASE(\theta_s,\theta_v,\phi)$ so as to extrapolate it onto a standard configuration of observation. This standard configuration corresponds to an observation at nadir with a solar zenith angle θ_s^0 of 40°. This particular θ_s^0 value was chosen because it roughly corresponds to the average of the illumination angles inferred from the database. Note that such a normalization procedure was preferred to the simple use of the k_0 parameter because the latter corresponds to a reflectance that would be measured under a very specific illumination situation which is never fulfilled for most sites (at nadir and for a sun at the zenith); it is therefore more subject to extrapolation errors when the actual illumination direction departs from it.

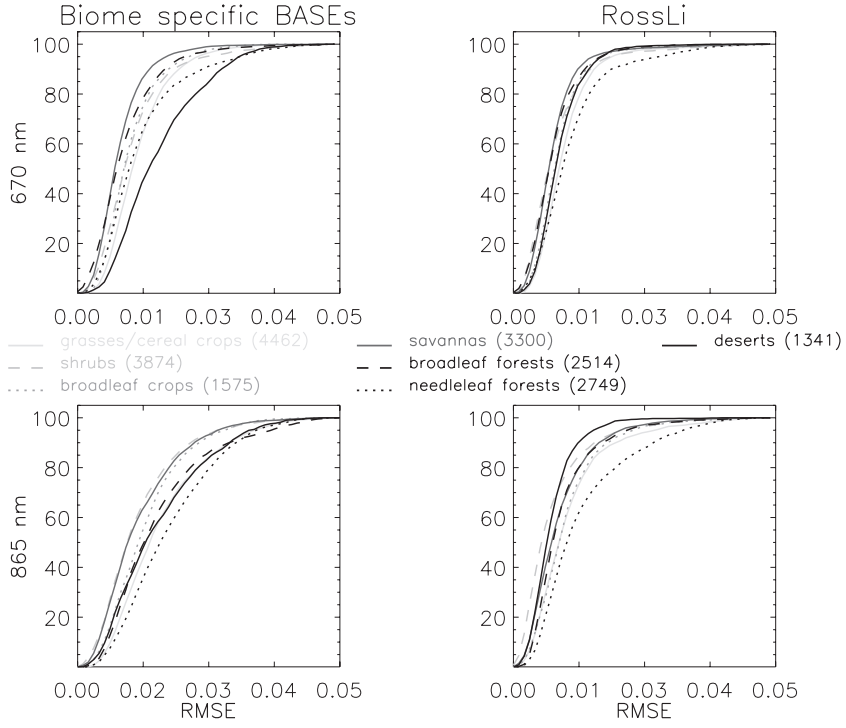

Fig. 9. Cumulative histograms of the RMSEs of fit considering the biome specific BASEs (left) and the three parameter Ross–Li model (right) at 670 and 865 nm. The number of sites considered by biome are given in brackets.

For a given target, the error of normalization (EoN) is defined as the root mean square error between the normalized reflectances, determined for each observation, and the "true" reflectance value in the standard configuration. Because this value is not known, it is determined from the full BRDF model, the three parameters of which being estimated from all measurements of the target. The comparison of the reflectances corrected with the biome specific BASEs and the "true" ones shows no significant bias and the distribution of the points along the one-to-one line has a noise-like pattern (results not shown). The EoN only slightly exceed the error of fit discussed in Section 4.2. As each individual measurement is taken independently from the others, the computation of the normalization error is indeed more sensitive to reflectance fluctuations, due both to measurement noise and variation of the target reflectance within the period of synthesis, than the error of fit, the determination of which explicitly minimizes the variance of the measurements around the a priori directional surface.

The purpose of normalization aims at inferring a reflectance corrected of the bidirectional effects, which amounts to reduce the reflectance variability. The error of normalization thus quantifies the residual variance after correction: the lower it is, the more efficient the normalization is. One cannot expect of a normalization procedure based on such a priori directional shapes to perform better than an approach relying on a BRDF fitted on a full dataset. Conversely, it must significantly reduce the actual reflectance variability to be valuable. These aspects are examined by comparing the reflectance variability (i) when no normalization is performed, (ii) after normalization based on a single BASE for all biome types, (iii) after normalization using the biome specific BASE.

The mean standard deviation of the observations $\sigma(R_{\mathrm{obs}})$ quantifies, for a given biome type, the variability of the remote sensed data due mainly to the surface reflectance anisotropy (and to a lesser extent to observational noise and temporal variation). $\sigma(R_{\mathrm{obs}})$ corresponds to the error made when considering the surface as Lambertian: it is on average of 0.02 in the red and of 0.04 in the near infrared. The normalization procedure reduces that variability by a factor 2 and 3, respectively, as attested by the values of the EoN. As expected, and even though the differences are generally slight, it performs better when using BASEs dedicated to each vegetation types instead of a single one, in particular for the unvegetated areas. The benefits gained are the more prominent in the near infrared in general and for the forest biomes in particular. The residual error is explained, by the variability of the BRDF shapes, and also the measurement errors. The results show that the EoN exceeds only slightly the error of fit for the three-parameter model. Thus, an a priori BASE is almost as good as an inverted BRDF to normalize the measurements. It thus supports the proposed methodology.

5. Summary and conclusion

The rich archive of POLDER-1 measurements was analyzed to determine the relationships between vegetation cover types and their directional signature. To account for the large range of observation geometries, the BRDF dimensionality was reduced to that of the three empirical coefficients of the Ross–Li model, modified to account for the hot spot effect within turbid media. Their dependency with biome type, in the red and near infrared, was investigated using the MODIS classification map that discriminates the Earth surface into seven vegetation classes: (1) grasses and cereal crops, (2) shrubs, (3) broadleaf crops, (4) savannas, (5) broadleaf forests, (6) needleleaf forests, and (7) deserts. The results have demonstrated only weak relationships between biome type and BRDF features, indicating that the angular information carries little information for biome categorization. The biome discernability is more pronounced in the spectral space of the observations, even when no temporal evolution of their optical properties was explicitly accounted for. The high variability of the directional coefficients for each biome class likely traduces the diversity in structural situations.

The different Earth landsurfaces were found to exhibit similar bidirectional reflectance features that translate in magnitude depending on the leaf and soil optical properties. Consequently, a standard parameterisation of their BRDF was proposed. It was defined for each of the MODIS biome classes. Then, a Bidirectional Anisotropy Standard shapE (BASE) models a biome specific BRDF as a function of a single spectral parameter only, that can be adjusted from any reflectance measurement. The average error of fit using the BASEs is of the order of 10% in the red and 5% in the near infrared, all biome type included. It proves the ability of these a priori directional surfaces to satisfactorily reproduce the observed directional signatures. The use of such standard BASEs requires a sole measurement, thus offering the possibility to correct operationally radiometric data acquired by single angle instruments from the bidirectional effects. The results indicate that the a priori BASEs can be used to normalize the reflectance measurements and decrease the variability due to directional effects by a factor greater than 2. We are currently using these BASEs for the correction of NOAA/AVHRR reflectance time-series at 8 km spatial resolution for studying long-term carbon fluxes by assimilation in the ORCHIDEE (Organizing Carbon and Hydrology In Dynamic Ecosystems Environment) ecophysiological model (Viovy et al., 2001).

References

Asner, G. P. (2000). Contributions of multi-angle remote sensing of land-surface and biogeochemical research. *Remote Sensing Reviews*, *18*, 137–162.

Bacour, C., Jacquemoud, S., Leroy, M., Hautecoeur, O., Weiss, M., & Prévot, L., et al. (2002). Reliability of the estimation of vegetation characteristics by inversion of three canopy reflectance models on airborne POLDER data. *Agronomie Agriculture and Environment*, *22*, 555–565.

Bicheron, P., & Leroy, M. (2000). Bidirectional reflectance distribution function signatures of major biomes observed from space. *Journal of Geophysical Research*, *105*(21), 26669–26681.

Bicheron, P., Leroy, M., Hautecoeur, O., & Bréon, F.-M. (1997). Enhanced discrimination of boreal forest covers with directional reflectances from the airborne polarization and directionality of the Earth reflectances (POLDER) instrument. *Journal of Geophysical Research*, *102*, 29517–29528.

Braswell, B. H., Schimel, D. S., Linder, E., & Moore III, B. (1997). The response of global terrestrial ecosystems to interannual temperature variability. *Science*, *278*, 870–872.

Bréon, F.-M., & Colzy, S. (1999). Cloud detection from the spaceborne POLDER instrument and validation against surface synoptic observations. *Journal of Applied Meteorology*, *38*, 777–785.

Bréon, F.-M., Maignan, F., Leroy, M., & Grant, I. (2002). Analysis of hot spot directional signatures measured from space. *Journal of Geophysical Research*, *107*(16), 4282–4296.

Briottet, X., Hosgood, B., Meister, G., Sandmeier, S., & Serrot, G. (2004). Laboratory measurements of bi-directional reflectance. In X. Schönemark, Geiger, & Röser (Eds.), *Reflection properties of vegetation and soil — With a BRDF data base* (pp. 173–194). Berlin: Wissenschaft und Technik Verlag.

Camacho de Coca, F., Bréon, F.-M., Leroy, M., & Garcia-Haro, F. J. (2004). Airborne measurements of hot spot reflectance signatures. *Remote Sensing of Environment*, *90*, 63–75.

Chen, J. M., Liu, J., Leblanc, S. G., Lacaze, R., & Roujean, J.-L. (2003). Multi-angular optical remote sensing for assessing vegetation structure and carbon absorption. *Remote Sensing of Environment*, *84*, 516–525.

Cihlar, J., Ly, H., Li, Z., Chen, J., Pokrant, H., & Huang, F. (1997). Multitemporal, multichannel AVHRR data sets for land biosphere studies — Artifacts and corrections. *Remote Sensing of Environment*, *60*, 35–57.

Csiszar, I., Gutman, G., Romanov, P., Leroy, M., & Hautecoeur, O. (2001). Using ADEOS/POLDER data to reduce angular variability of NOAA/AVHRR reflectances. *Remote Sensing of Environment*, *76*(3), 399–409.

Deering, D. W., & Leone, P. (1986). A sphere-scanning radiometer for rapid directional measurements of sky and ground radiance. *Remote Sensing of Environment*, *19*, 1–24.

d'Entremont, R. P., Schaaf, C. B., Lucht, W., & Strahler, A. H. (1999). Retrieval of red spectral albedo and bidirectional reflectance using AVHRR HRPT and GOES satellite observations of the New England region. *Journal of Geophysical Research*, *104*(D6), 6229–6239.

Deschamps, P. Y., Bréon, F.-M., Leroy, M., Podaire, A., Bricaud, A., & Buriez, J. C., et al. (1994). The POLDER Mission: Instrument characteristics and scientific objectives. *IEEE Transactions on Geoscience and Remote Sensing*, *2*(3), 598–615.

Diner, D. J., Asner, G. P., Davies, R., Knyazikhin, Y., Muller, J.-P., & Nolin, A. W., et al. (1999). New directions in Earth observing: Scientific applications of multiangle remote sensing. *Bulletin of the American Meteorological*, 2209–2228.

Duchemin, B. (1999). NOAA/AVHRR bidirectional reflectance: Modeling and application for the monitoring of a temperate forest. *Remote Sensing of Environment*, *67*, 51–67.

Gao, F., Schaaf, C. B., Strahler, A. H., Jin, Y., & Li, X. (2003). Detecting vegetation structure using a kernel-based BRDF model. *Remote Sensing of Environment*, *86*, 198–205.

Garrigues, S., Allard, D., & Baret, F., submitted for publication. Characterisation of landscape spatial heterogeneity through remote sensing data. *Remote Sensing of Environment*.

Gemmell, F. (2000). Testing the utility of multi-angle spectral data for reducing the effects of background spectral variations in forest reflectance model inversion. *Remote Sensing of Environment*, *72*, 46–63.

Gerstl, S. A. W., Simmer, C., & Power, B. J. (1986). The canopy hot spot as canopy identifier. *Symposium on remote sensing of resources development and environment management* (pp. 261–263). Netherlands: Enschede.

Hautecoeur, O., & Leroy, M. (1998). Surface bidirectional reflectance distribution function observed at global scale by POLDER/ADEOS. *Geophysical Research Letters*, *25*(22), 4197–4200.

Khlopenkov, K., Trishchenko, A. P., & Luo, Y. (2004). Analysis of BRDF and albedo properties of pure and mixed surface types from Terra MISR using Landsat high-resolution land cover and angular unmixing technique. *Fourteenth ARM science team meeting proceedings, Albuquerque, New Mexico, March 22–26*. 9 pp.

Kimes, D. S. (1983). Dynamics of directional reflectance factor distribution for vegetation canopies. *Applied Optics*, *22*, 1364–1372.

Knyazikhin, Y., Glassy, J., Privette, J. L., Tian, Y., Lotsch, A., & Zhang, Y., et al. (1999). *MODIS leaf area index (LAI) and fraction of photosynthetically active radiation absorbed by vegetation (FPAR) product (MOD15) — Algorithm theoretical basis document*. http://cybele.bu.edu/modismisr/atbds/modisatbd.pdf, 130 pp.

Kriebel, K.T., 1977. Reflection properties of vegetated surfaces: Tables of measured spectral biconical reflectance factors. Münchener Universitäts-Schriften, Fachbereich Physik, Nr. 29.

Lacaze, R., 2003. POLDER-1 BRDF database — User document. Available at: http://medias.obs-mip.fr/postel/Projets/POLDER/produits/polder1/brdf.

Lacaze, R., Chen, J. M., Roujean, J.-L., & Leblanc, S. G. (2002). Retrieval of vegetation clumping index using hot spot signatures measured by POLDER instrument. *Remote Sensing of Environment*, *79*, 84–95.

Leroy, M., & Bréon, F.-M. (1996). Angular signatures of surface reflectances from airborne POLDER data. *Remote Sensing of Environment*, *57*, 97–107.

Leroy, M., Deuzé, J. L., Bréon, F. M., Hautecoeur, O., Herman, M., & Buriez, J. C., et al. (1997). Retrieval of atmospheric properties and surface bidirectional reflectances over land from POLDER/ADEOS. *Journal of Geophysical Research*, *102*, 17023–17037.

Leroy, M., & Roujean, J. L. (1994). Sun and view angle corrections on reflectances derived from NOAA/AVHRR data. *IIEEE Transactions on Geoscience and Remote Sensing*, *32*, 684–697.

Liang, S., Strahler, A. H., Jin, X., & Zhu, Q. (1997). Comparisons of radiative transfer models of vegetation canopies and laboratory measurements. *Remote Sensing of Environment*, *61*, 129–138.

Lovell, J. L., & Graetz, R. D. (2002). Analysis of POLDER-ADEOS data over the Australian continent: The relationship between BRDF and vegetation structure. *International Journal on Remote Sensing*, *23*(14), 2767–2796.

Lu, H., Raupach, M. R., McVicar, T. R., & Barrett, D. J. (2003). Decomposition of vegetation cover into woody and herbaceous components using AVHRR NDVI time series. *Remote Sensing of Environment*, *86*(1), 1–18.

Lucht, W., Schaaf, C. B., & Strahler, A. H. (2000). An algorithm for the retrieval of albedo from space using semiempirical BRDF models. *IEEE Transactions on Geoscience and Remote Sensing*, *38*, 977–998.

Maignan, F., Bréon, F.-M., & Lacaze, R. (2004). Bidirectional reflectance of Earth targets: Evaluation of analytical models using a large set of spaceborne measurements with emphasis on the hot spot. *Remote Sensing of Environment*, *90*, 210–220.

Maisongrande, P., Ruimy, A., Dedieu, G., & Saugier, B. (1995). Monitoring seasonal and interannual variations of gross primary productivity, net primary productivity and net ecosystem productivity using a diagnostic model and remotely-sensed data. *Tellus*, *47*(B), 178–190.

Marticorena, B., Chazette, P., Bergametti, G., Dulac, F., & Legrand, M. (2004). Mapping the aerodynamic roughness length of desert surfaces

from the POLDER/ADEOS bi-directional reflectance product. *International Journal of Remote Sensing*, *25*(3), 603–626.

McCloy, K. R., & Lucht, W. (2004). Comparative evaluation of seasonal patterns in long time series of satellite image data and simulations of a global vegetation model. *IEEE Transactions on Geoscience and Remote Sensing*, *42*(1), 140–153.

Myneni, R. B., Keeling, C. D., Tucker, C. J., Asrar, G., & Nemani, R. R. (1997). Increased plant growth in the northern high latitudes from 1981 to 1991. *Nature*, *386*, 698–702.

Pinty, B., Widlowski, J.-L., Gobron, N., Verstraete, M., & Diner, D. J. (2002). Uniqueness of multiangular measurements — Part I: An indicator of subpixel surface heterogeneity from MISR. *IEEE Transactions on Geoscience and Remote Sensing*, *40*(7), 1560–1573.

Rock, B. N., Williams, D. L., Moss, D. M., Lauten, G. N., & Kim, M. (1994). High-spectral resolution field and laboratory optical reflectance measurements of red spruce and eastern hemlock needles and branches. *Remote Sensing of Environment*, *47*, 176–189.

Ross, J. (1981). *The radiation regime and architecture of plant stands*. The Hague, Netherlands: Dr Junk Publishers. 392 pp.

Roujean, J. L., Leroy, M., & Deschamps, P. Y. (1992). A bidirectional reflectance model of the Earth's surface for the correction of remote sensing data. *Journal of Geophysical Research*, *97*, 20455–20468.

Running, S., & Nemani, R. R. (1988). Relating seasonal patterns of the AVHRR vegetation index to simulated photosynthesis and transpiration of forests in different climates. *Remote Sensing of Environment*, *24*, 347–367.

Sandmeier, S. (1999). Acquisition of bidirectional reflectance factor data with field goniometers. *Remote Sensing of Environment*, *73*, 257–269.

Solheim, I., Engelsen, O., Hosgood, B., & Andreoli, G. (2000). Measurements and modeling of the spectral and directional reflection properties of lichen and moss canopies. *Remote Sensing of Environment*, *72*, 78–94.

Tsay, S. C., King, M. D., Arnold, G. T., & Li, J. Y. (1998). Airborne spectral measurements of surface anisotropy during SCAR-B. *Journal of Geophysical Research*, *103*, 31943–31953.

Viovy, N., François, C., Bondeau, A., Krinner, G., Polcher, J., & Kergoat, L., et al. (2001). Assimilation of remote sensing measurements into the ORCHIDEE/STOMATE DGVM biosphere model. *Proceedings 8th international symposium physical measurements and signatures in remote sensing, 8–12 January, Aussois, (France)* (pp. 713–718).

Wanner, W., Li, X., & Strahler, A. H. (1995). On the derivation of kernels for kernel-driven models of bidirectional reflectance. *Journal of Geophysical Research*, *100*(D10), 21077–21089.

Williams, D. L. (1991). A comparison of spectral reflectance properties at the needle, branch, and canopy level for selected conifer species. *Remote Sensing of Environment*, *35*, 79–93.

Wu, A., Li, Z., & Cihlar, J. (1995). Effects of land cover type and greenness on advanced very high resolution radiometer bidirectional reflectances: Analysis and removal. *Journal of Geophysical Research*, *100*(D5), 179–9192.

Zhang, Y., Tian, Y., Myneni, R. B., Knyazikhin, Y., & Woodcock, C. E. (2002). Assessing the information content of multiangle satellite data for mapping biomes. I. Statistical framework. *Remote Sensing of Environment*, *80*, 418–434.